**Journal of Applied and Computational Mechanics**

Research Paper

# Scalings of Inverse Energy Transfer and Energy Decay in 3-D Decaying Isotropic Turbulence with Non-rotating or Rotating Frame of Reference

## Rou Chen[1], Huidan (Whitney) Yu[1], Yousheng Xu[2], Luoding Zhu[3]

[1] Department of Mechanical & Energy Engineering, Indiana University-Purdue University Indianapolis, Indianapolis, IN 46202, USA

[2] School of Light Industry, Zhejiang University of Science and Technology, Hangzhou 310023, China

[3] Department of Mathematical Sciences, Indiana University-Purdue University Indianapolis, IN 46202, USA

**Abstract.** Energy development of decaying isotropic turbulence in a 3-D periodic cube with non-rotating or rotating frames of reference is studied through direct numerical simulation using GPU accelerated lattice Boltzmann method. The initial turbulence is isotropic, generated in spectral space with prescribed energy spectrum $E(\kappa) \sim \kappa^m$ in a range between $\kappa_{min}$ and $\kappa_{max}$. The Taylor microscale Reynolds number $Re_\lambda$ and Rossby number $Ro$ are introduced to characterize the inertial, viscous, and rotational attributes of the system. The focus of this study is on the scalings of early inverse energy transfer and late energy decay in the development of turbulent energy under various conditions through combinations of $m$, $\kappa_{min}$, $\kappa_{max}$, $Re_\lambda$ and $Ro$. First, we demonstrate the validity of the simulation by confirming the quantitative dependence of the decay exponent $n$ on the initial energy spectrum exponent $m$, at $Re_\lambda$ =255 and $Ro=\infty$, varying the values of $m$, $\kappa_{min}$ and $\kappa_{max}$. Second, at relatively low $Re_\lambda$, the decay exponent for different initial spectra statistically fall in respective ranges, all of which agree well with the corresponding analytical predictions. Third, we quantitatively investigate the 3-D inverse energy transfer. Our findings include (i) the exponent of inverse energy transfer spectrum $E(\kappa) \sim \kappa^\sigma$ depends on the initial spectrum exponent $E(\kappa) \sim \kappa^m$: if $m<4$, $\sigma=m$ while if $m \geq 4$, $\sigma=4$; (ii) rotation alters the inverse energy transfer rate when $Re_\lambda \leq 255$ and $Ro \geq 0.8$; (iii) the energy increase in large scale during inverse energy transfer exhibits a bell shape, the peak of which varies with $Re_\lambda$ and $Ro$.

**Keywords:** Inverse energy transfer; Decaying isotropic turbulence; Rotational turbulence; Lattice Boltzmann method; GPU parallel computation

## 1. Introduction

Owing to the highly nonlinear interactions among a wide range of motion scales in space and time, turbulent flow remains unresolved even for canonical cases such as isotropic turbulence in a periodic box. Since the seminal studies of Birkhoff, Batchelor and Saffman [1-4], decaying isotropic turbulence (DIT) has been the subject of many experimental and numerical studies. There exist two canonical cases in wave space $\kappa(\kappa_x, \kappa_y, \kappa_z; \kappa=|\kappa|)$ in terms of energy spectrum in low wave number: $E(\kappa \to 0) \sim L\kappa^2$ and $E(\kappa \to 0) \sim I\kappa^4$, in which $L=\int <\boldsymbol{u(x)} \cdot \boldsymbol{u(x+r)}> d\boldsymbol{r}$ and $I=-\int r^2 <\boldsymbol{u(x)} \cdot \boldsymbol{u(x+r)}> d\boldsymbol{r}$ are Birkhoff [2] and Loitsyansky [5] integrals respectively. Whether turbulence is of Batchelor ($E \sim \kappa^4$) or Saffman ($E \sim \kappa^2$) type depends on the initial condition: for a turbulence is initially scaled with $\kappa^m$, it stays with $\kappa^2$ if $m=2$ while stays with $\kappa^4$ if $m \geq 4$ [6]. The relevant flow invariant, asymptotic decay exponent and the low wave-number scaling are strongly affected by the initial spectrum and Reynolds number.

Published online: April 30 2019

Isotropic turbulence is typically characterized by the Taylor-microscale Reynolds number defined as

$$\mathrm{Re}_{\lambda} = \frac{u_{rms}\lambda}{\nu} = 2k\sqrt{\frac{5}{3\nu\varepsilon}} \tag{1}$$

where $\lambda(=(\sqrt{15\nu u_{rms}^2/\varepsilon}))$ is the transverse Taylor-microscale length, $u_{rms}(=\sqrt{2k/3})$ is the root mean square (rms) of the velocity field $\boldsymbol{u}$, $k(=\int E(\kappa)d\kappa)$ is the kinetic energy, $\epsilon(=\int 2\nu\kappa^2 E(\kappa)d\kappa)$ is the dissipation rate of the kinetic energy, and $\nu$ is the kinematic viscosity of the fluid. The energy spectrum $E(\kappa, t)$ in DIT evolves as $\partial_t E(\kappa,t) = -T(\kappa,t) - 2\nu\kappa^2 E(\kappa, t)$ where $T(\kappa,t)$ represents the nonlinear energy transfer between Fourier modes (cf. Eq. (6.162) in [7]). It has been long observed that, after a short initial transient period, the kinetic energy $k$ exhibits power-law decays as $k(t)/k_0 \sim (t/t_0)^{-n}$ where $k_0$ is the value of $k$ at a reference time $t_0$ (cf. Eq. (5.274) in [7]). We use $t'$ to denote $t/t_0$ in Section 3 below for results and discussion. The value of decay exponent $n$ depends on the value of initial energy spectrum exponent $m$ when initial $Re_\lambda$ is sufficiently high. In specific, the relationship between $n$ and $m$ can be theoretically derived from a transformation of dynamical variables based on invariance of a physical state and dimensional analysis, $n=4/3$ for $m=3$ [8], and $n=10/7$ when $m=4$ [9].

When the system is subject to a rotating frame of reference with an angular velocity $\boldsymbol{\Omega}$, Coriolis force, which is linear in the velocity, modifies the nonlinear dynamics of the turbulent flow. The flow evolves with a SLOW scale $\tau_L \sim L/U$ associated with eddies at a characteristic scale $L$ ($U$ is a characteristic velocity) and a FAST scale $\tau_\Omega \sim 1/|\boldsymbol{\Omega}| \sim \tau_L Ro$ associated with the rotation. The dimensionless Rossby number $Ro$ is defined as

$$Ro = \frac{u_{rms}}{2|\boldsymbol{\Omega}|L} \tag{2}$$

Where $L = 2\pi\sum_{\kappa}\kappa^{-1}E(\kappa)/\sum_\kappa E(\kappa)$ is the integral length of the turbulence. The $Ro$ number, which decreases when rotation increases, measures the influence of rotation on the nonlinear dynamics of turbulence. Thus the dynamics of DIT becomes significantly richer.

It has been reported that turbulent energy decay rate of $\kappa^4$ is reduced from -10/7 (without rotation) to -7/5 (with strong enough rotation) [9]. In the presence of rotation, energy decay is slowed down due to the energy transfer towards two-dimensional (2-D) slow modes [10,11]. The development of anisotropy and reduction of the energy transfer have been verified in numerical simulations [12-16] and experiments [17,18]. Recently, Teitelbaum and Mininni [9] systematically studied the decay of turbulence in rotating flow focusing on various effects, such as the initial energy spectrum exponent, helicity, $Ro$ number, and $Re$ number.

Energy cascade transfers energy continuously from larger scale motions to smaller scale motions until sufficiently small length scales with which viscous forces dissipate energy into heat. This is a basic phenomenology of turbulence proposed by Richardson [19]. Whereas inverse energy transfer from smaller scales to larger scales has been observed in two-dimensional (2-D) turbulence [20-23] but rarely observed in three-dimensional (3-D) turbulence unless there exists strong anisotropy [24-28] or rotation [29-31]. Recently, it has been demonstrated [32] that all 3-D flows in nature possess a subset of nonlinear evolution leading to a reverse energy transfer.

The present study is a part of our continuous efforts to investigate the underlying physics of DIT with and without rotation using lattice Boltzmann method (LBM) [33,34]. We have previously developed the LBM for direct numerical simulation (DNS) and large eddy simulation (LES) for DIT [35,36]. Recently we implemented GPU acceleration of the LBM for the DNS of DIT and demonstrated the computational efficiency and physical validity [37]. The computation is significantly accelerated; achieving over 300 times speed up than the serial code. Using the developed GPU-LBM, we are now able to systematically study the energy development of DIT. The initial isotropic turbulence is generated in Fourier spectral space with prescribed energy spectrum $E(\kappa) \sim \kappa^m$ in a range between $\kappa_{min}$ and $\kappa_{max}$. The Taylor microscale Reynolds number $Re_\lambda$ and Rossby number $Ro$ are introduced to characterize the inertial, viscous, and rotational attributes of the system. The focus of this study is on the scalings of early inverse energy transfer during the early transient stage and late asymptotic energy decay in the development of turbulent energy under various conditions through the combination among $m$, $\kappa_{min}$, $\kappa_{max}$, $Re_\lambda$, and $Ro$.

The remainder of the paper is organized as follows. In Section 2, we briefly introduce the numerical tool, i.e. LBM, and initial and boundary conditions. Physical results are presented in Section 3. Finally, Section 4 provides a summary discussion and concludes the paper.

## 2. Lattice Boltzmann Method and Computational Set-up

The LBM has been developed as a reliable alternative to solve fluid dynamics especially for complex flow [38,39] in the last two decades. One of the most important advantages of the LBM is that its implementable data structure ideally fits the GPU (Graphic Processing Unit) architecture, leading to a dramatic acceleration of computation through GPU parallel computing [37,40]. This feature greatly promotes the capability of LBM to solve complex flow such as turbulence, which is expensive in both computation and memory.

The lattice Boltzmann equation reads

$$f_\alpha(\boldsymbol{x}+\boldsymbol{e}_\alpha\delta t, t+\delta t) = f_\alpha(\boldsymbol{x},t) - \frac{1}{\tau}[f_\alpha - f_\alpha^{eq}] + F_\alpha \tag{3}$$

Where $f_\alpha$ is the single-partial distribution with discrete molecular velocity $\boldsymbol{e}_\alpha$ and $\tau$ is the relaxation time caused by molecular collision. In this work, we employ the 3D 19-velocity (D3Q19) model due to its reliability and efficiency of computation [41], thus $\alpha=0,1,\cdots,18$. The corresponding discrete velocity sets $\boldsymbol{e}_\alpha$ are $(0,0)$ for $\alpha=0$; $(\pm1,0,0)c$, $(0,\pm1,0)c$, $(0,0,\pm1)c$ for $\alpha=1\sim6$; and

$(\pm1,\pm1,0)c$, $(0,\pm1,\pm1)c$, $(\pm1,0,\pm1)c$ for $\alpha=7\sim18$. The parameter $c$ is the lattice velocity defined as $c=\delta x/\delta t$ with $\delta x$ the lattice length and $\delta t$ the time step. In practice, $c$, $\delta x$, and $\delta t$ are usually set to 1. The equilibrium distribution function $f_\alpha^{eq}$ is formulated [42] as

$$f_\alpha^{eq} = \omega_\alpha \{\delta\rho + \rho_0[\frac{3e_\alpha \cdot u}{c^2} + \frac{9(e_\alpha \cdot u)^2}{2c^4} - \frac{3u^2}{2c^2}]\} \tag{4}$$

where $\omega_\alpha$ is the weight coefficient, in D3Q19, $\omega_0=1/3$, $\omega_{1-6}=1/18$, $\omega_{7-18}=1/36$. The density $\rho=\rho_0+\delta\rho$ with $\rho_0$ the mean density in the system and $\delta\rho$ the fluctuation of density. The force term $F_\alpha$ is the discrete format [43] of the Coriolis force (per mass) a as:

$$F_\alpha = -3\omega_\alpha\rho_0\frac{e_\alpha \cdot a}{c^2}\delta t \tag{5}$$

Through the Chapman-Enskog expansion [44], it has been proved that the lattice Boltzmann evolution equation (Eq. 3) recovers Naiver-Stokes equations in incompressible limit [42].

$$\nabla \cdot u = 0 \tag{6}$$

$$\frac{\partial u}{\partial t} + u \cdot \nabla u = -\nabla p + \nu\nabla^2 u + a \tag{7}$$

where $p$ is the pressure which presents as $p=c_s^2\rho/\rho_0$ with $c_s$ the sound speed of the model which is equal to $c/\sqrt{3}$. It is noted that the kinematic viscosity $\upsilon$ is the viscosity associated with the relaxation time $\tau$ as $\upsilon=c_s^2(\tau-1/2)$.

The simulations are conducted in a 3-D periodic cube. In the case of rotation, we introduce Coriolis force a as the external force in Eq. (3). The Coriolis force is characterized by $a=-2\Omega\times u$, where $\Omega=\Omega_z k$ is the angular velocity of the rotation. This force is discretized through Eq. (5). The initial incompressible isotropic velocity field $u(x,0)$, which satisfies $\nabla\cdot u(x,0) = 0$ is generated in spectral space $\kappa$ with the following energy spectrum in a prescribed range $\kappa_{min}\leq\kappa\leq\kappa_{max}$ and a random phase (cf. details in [45]):

$$E(\kappa,0) = \begin{cases} \alpha\kappa^m e^{-0.14\kappa^2} & \kappa \in [\kappa_{min}, \kappa_{max}] \\ 0 & \kappa \in [\kappa_{min}, \kappa_{max}] \end{cases} \tag{8}$$

in which $m$ is an adjustable integer characterizing the spectrum exponent and $\alpha$ is a parameter to adjust the magnitude of the velocity field. It is noted that $m=2$ and $m=4$ correspond to Birkhoff and Loitsyansky cases mentioned in Section 1.

## 3. Results and Discussion

The GPU-LBM simulation is carried out on two local workstations: one is with 2 CPUs (Intel Xeon E5645/64 GB memory/2.40 GHz/Quad-Core) and a Tesla M2090 6GB memory GPU card with ECC enabled by default and another with 12 CPUs (Intel E5660/49 GB memory/2.80GHZ/double-Core) and 4 Tesla C2075 6GB memory GPU cards. The flow domain is a periodic cube with resolution of $256^3$ subject to a rotation in z-direction. We study a variety of cases using 8 values of $Re_\lambda$ from 75 to 255, 4 values of $m$ from 3 to 6, and 2 $\kappa$ ranges of $1\leq\kappa\leq8$ and $8\leq\kappa\leq16$ of the initial turbulence. For rotation, we have 3 values of $Ro$, 0.8, 3, and $\infty$, for the reference rotation. Quantitative effects of $Re_\lambda$, $m$, and $Ro$ under the two $\kappa$ ranges on the development of DIT are present below in two aspects.

### 3.1. Scaling of asymptotic kinetic energy decay

We first present the dependence of decay exponent $n$ on the initial energy spectrum exponent $m$ with no rotation ($\Omega_z=0$ or $Ro=\infty$). The energy decay of $k/k_0$ at $m=3$, 4 are shown in Fig. 1(a), (b) respectively, each of which has two $\kappa$ ranges, $1\leq\kappa\leq8$ with $Re_\lambda=255$ (solid line) and $8\leq\kappa\leq16$ with $Re_\lambda=128$(dashed line). The corresponding decay exponents (scaled by a dash-dot line in each plot) for the two cases are (a) 4/3, (b) 10/7 respectively. These decay exponents are in good agreement with the corresponding ones predicted [8,9], demonstrating the validity of the LBM simulation.
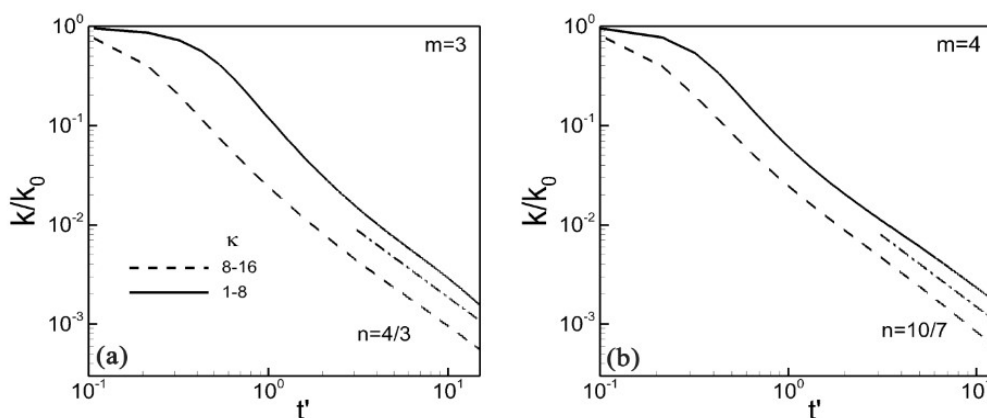


**Fig. 1.** Dependence of decay exponent $n$ of kinetic energy on initial energy spectrum exponent from GPU-LBM simulation. The values of $m$ are (a) 3, (b) 4. Solid lines: $1\leq\kappa\leq8$ and $Re_\lambda=255$; dashed line: $8\leq\kappa\leq16$ and $Re_\lambda=128$

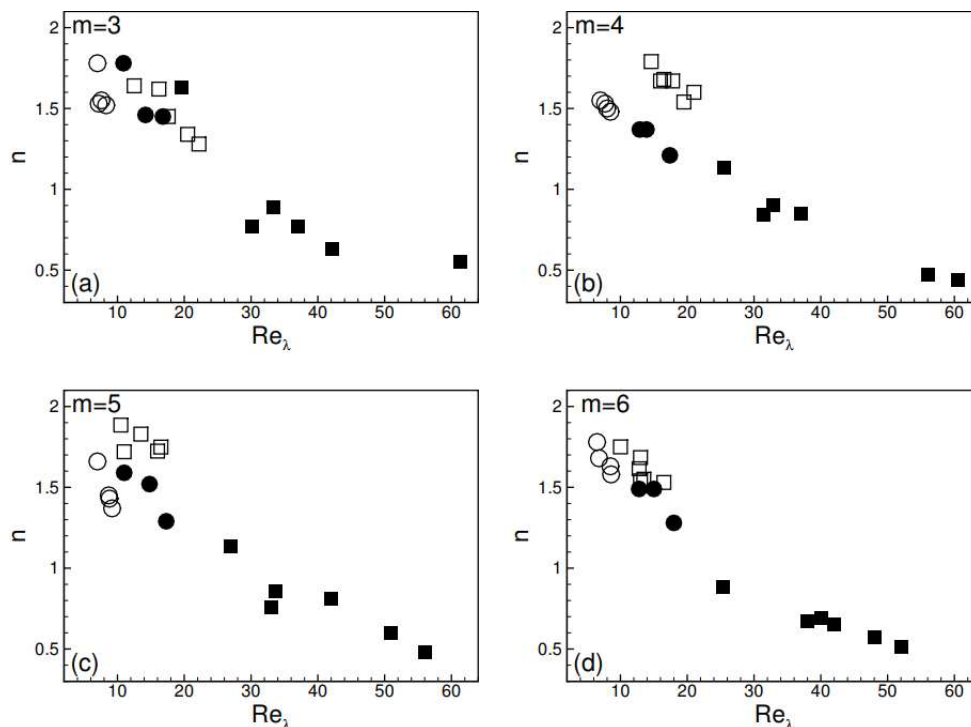**Fig. 2.** Dependence of the decay exponent $n$ on $Re_\lambda$ with 4 values of $m$: (a) $m=3$, (b) $m=4$, (c) $m=5$, and (d) $m=6$. Without rotation ($Ro=\infty$): empty symbols. With rotation ($Ro=0.8$): filled symbols. $1\leq \kappa \leq 8$: squares; $8\leq \kappa \leq 16$: circles.

It has been reported that the decay exponent varies when the $Re_\lambda$ is relatively low, e.g. $Re_\lambda<30$ [35,46,47]. Here we study the dependency of the decay exponent $n$ on $Re_\lambda$ in a range of low $Re_\lambda$ from 7 to 60 with the initial $Re_\lambda$ from 75 to 255. As shown in Fig. 2, four values of $m$ from 3 to 6 are used. Each of them has two $\kappa$ ranges, 1-8 (squares) and 8-16 (circles), and two rotation conditions, without rotation ($Ro=\infty$, empty symbols) and with certain rotation ($Ro=0.8$, filled symbols). Without rotation, the decay exponent $n$ statistically falls in the ranges of 1.33-1.68, 1.48-1.67 for $m=3$, 4 respectively, consistent to the corresponding analytical predictions of $n=1.33$, 1.43 respectively. Meanwhile, $n$ falls in the ranges of 1.40-1.89 and 1.54-1.78 for $m=5$ and 6. In the studied range of $Re_\lambda$, variations of $n$ for different $Re_\lambda$ are seen in each $m$ case. A tendency that $n$ decreases as $Re_\lambda$ increases is well agreed with previous research [47-49]. The exponent is derived when $\lambda^2$ grows linearly in the decay region [47,48]. With rotation, the simulated $n$ falls in the ranges of 0.63-1.78, 0.80-1.37, 0.6-1.59, and 0.57-1.49 for $m=3$, 4, 5 and 6 respectively. The decay rate with rotation is smaller than those without rotation, which demonstrates that rotation prohibits kinetic energy decay [50]. The simulated results, filled squares in Fig. 2 are consistent with the analytical prediction.

### 3.2. Scaling of transient inverse energy transfer

In our previous study of DIT in a 3D periodic box [35], inverse energy transfer has been observed at the early stage of turbulence development after the large scale motion is injected in the box. As a follow up, here we quantitatively study the scaling of inverse energy transfer with and without rotation.

Inverse energy transfer is characterized by the energy transfer from smaller to larger motion scales as shown in Fig. 3. Two initial $\kappa^4$ ($m=4$) turbulent motions with $Re_\lambda =255$ and 128 are injected in the ranges of $1\leq \kappa \leq 8$ (left) and $8\leq \kappa \leq 16$ (right) respectively. No rotation is imposed. The backward scattering of kinetic energy occurs immediately after the initial turbulence is input and continues until the large scale motion is scaled as $E(\kappa) \sim \kappa^4$, i.e. the compensated energy spectrum becomes flat. When the initial energy is injected in the range of $1\leq \kappa \leq 8$ (left), inverse energy transfer makes the large scale motion ($1\leq \kappa \leq 8$) more energetic. In the case of the range $8\leq \kappa \leq 16$ (right) larger scale motion in the range of $1\leq \kappa \leq 8$ is seen, implying the occurrence of inverse energy transfer.

The flatness of a compensated energy spectrum $E(\kappa)/\kappa^\sigma$ is closely associated with the scaling of the initial energy spectrum $E(\kappa,0)\sim\kappa^m$. When $m\leq 4$, $\sigma$ equals to $m$, as seen in Fig. 3 for $m=4$ and Fig. 4(a), (b) for $m=3$. When $m>4$, $\sigma$ keeps the value of 4, as shown in Fig. 4(c), (d) and (e), (f) where $m=5$ and $m=6$ respectively. This is solid evidence to confirm an analytical prediction [8] that turbulence which starts as $\kappa^m$ ($m<4$) stays as $\kappa^m$ and turbulence which starts as $\kappa^4$ or steeper stays as $\kappa^4$ in the large motion scale.

In Fig. 5, we study the influence of rotation on the inverse energy transfer scaling. Again, initial $\kappa^4$ turbulent motions with $Re_\lambda$ values of 255 and 128 are injected in the ranges of $1\leq \kappa \leq 8$ (top row) and $8\leq \kappa \leq 16$ (bottom row) respectively. In the presence of a rotating frame of reference, $Ro=3$ in (a) and (c), and $Ro=0.8$ in (b) and (d). Inverse energy transfer is seen in each case but the transfer rate deviates from $m=4$. Rotation causes steeper inverse energy transfer when initial turbulence is injected in the largest motion scale $1\leq \kappa \leq 8$, whereas concentration of initial turbulence in the range of $8\leq \kappa \leq 16$ results in more gradual inverse energy transfer.
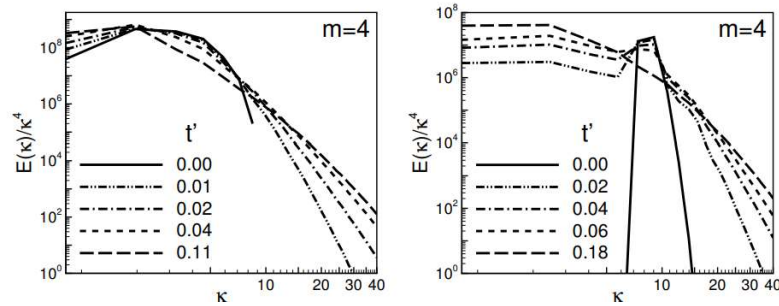
**Fig. 3.** Compensated energy spectra at different time in the early stage of DIT development with no rotation. Initial $\kappa^4$ ($m=4$) turbulent motions are injected in the range of $1 \le \kappa \le 8$ with $Re_\lambda = 255$ (left) and $8 \le \kappa \le 16$ with $Re_\lambda = 128$ (right). The inverse energy transfer stops when $E(\kappa)$ is scaled as $\kappa^4$.
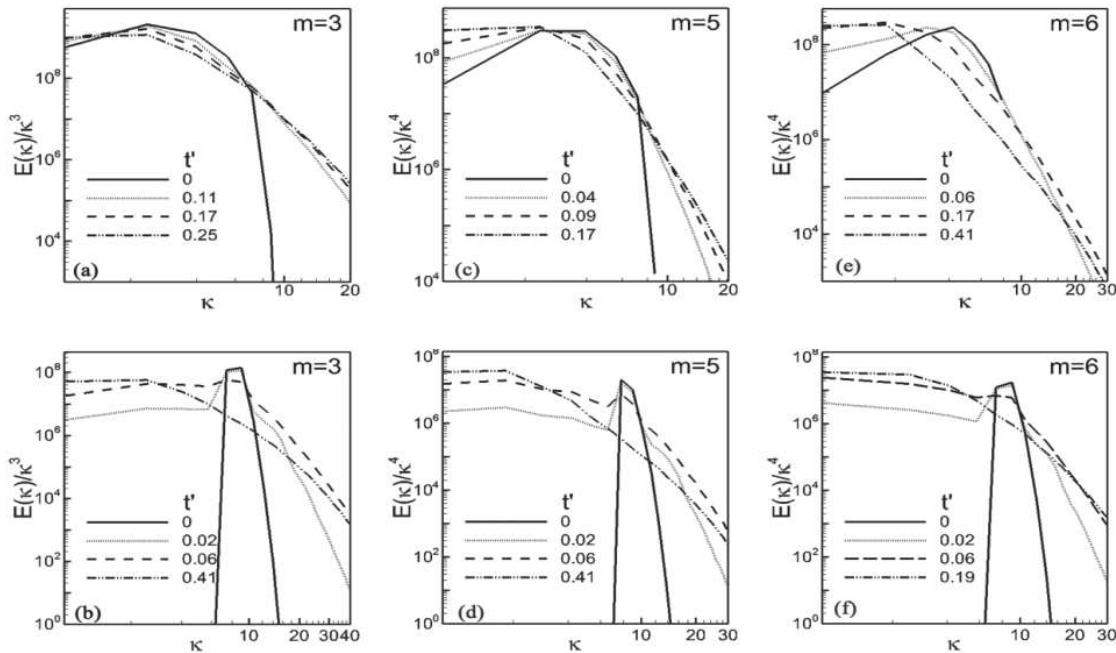


**Fig. 4.** Compensated energy spectra at different time in the early stage of energy transfer with no rotation. Initial $\kappa^m$ turbulent motions are injected in the range of $1 \le \kappa \le 8$ with $Re_\lambda = 255$ (top) and $8 \le \kappa \le 16$ with $Re_\lambda = 128$ (bottom) respectively. The values of $m$ are (a), (b) $m=3$, (c), (d) $m=5$, and (e), (f) $m=6$.
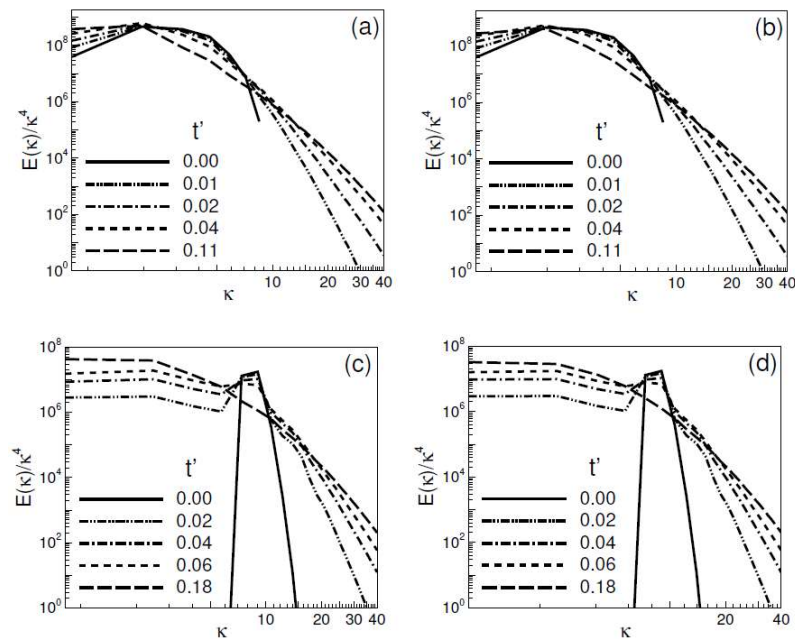


**Fig. 5.** Compensated energy spectra at early stage of turbulence development in the presence of rotation with $Re_\lambda = 255$ and $1 \le \kappa \le 8$ (top row) and $Re_\lambda = 128$ and $8 \le \kappa \le 16$ (bottom row). The values of $Ro$ are 3 for (a) and (c) and 0.8 for (b) and (d). Initial energy scales as $m=4$ for all the cases.

The amount of inverse energy transfer is quantitatively evaluated in Fig. 6. As illustrated in Fig. 6(a), the relative energy increase in the large scale area every five time steps is calculated from the area of $a$-$b$-$c$-$d$ at $t$ and area $e$-$b$-$c$-$d$ at $t+5$ as $\Delta E = (S_{ebcd} - S_{abcd})/S_{abcd}$. The time evolution of inverse transfer rate when the initial energy scales as $\kappa^4$ is shown in Fig. 6(b) with $Re_\lambda = 255$, $1 \le \kappa \le 8$. The inverse energy transfer exhibits two features. First, the inverse energy transfer rate, $\Delta E$, experiences a similar route starting with acceleration to a peak and then a deceleration. The peak varies with the turbulence and rotation conditions. Second, larger rotation (smaller $Ro$) has smaller inverse energy transfer rate, which is consistent with the observation that rotation prohibits the energy decay discussed above.
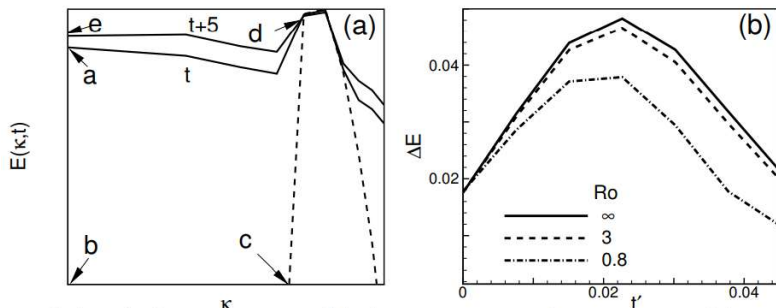


**Fig. 6.** Quantitative measurement of the inverse energy transfer amount every 5 time steps. (a) Illustration of the calculation of inverse energy transfer and (b) time evolution of the inverse energy transfer rate at $m=4$, $Re_\lambda=255$, $1 \le \kappa \le 8$.

## 4. Conclusions

Through the GPU-accelerated LBM simulation, we have studied energy transfer in the development of decaying turbulence. Simulations were carried out in a 3-D periodic cube with a resolution of $256^3$, subject to a rotating frame of reference with three rotational intensities that are $Ro=\infty$, 3, and 0.8. The initial incompressible isotropic turbulence was generated in spectral space with prescribed energy spectrum exponent $E(\kappa) \sim \kappa^m$, $m=3,4,5,6$, and injected in two ranges of Fourier mode, $1 \le \kappa \le 8$ and $8 \le \kappa \le 16$. The Taylor microscope Reynolds number $Re_\lambda$ varied from 75 to 255. We have focused on the decay exponent of kinetic energy in the late stage and on the scaling of inverse energy transfer in the early stage of turbulence development. The major results of this study are summarized as follows:

- The decay exponent deviates from the analytical prediction when $Re_\lambda$ is relatively low. The LBM simulated decay exponents for a large number of cases fall into ranges consistent with the theoretical predictions for different $m$ values.
- The scaling of the inverse energy transfer $E(\kappa) \sim \kappa^\sigma$ depends on the initial energy spectrum $E(\kappa) \sim \kappa^m$: $m<4$, $\sigma=m$ while if $m \ge 4$, $\sigma=4$.
- Energy increase in large scale during inverse energy transfer exhibits a bell shape starting with acceleration up to a peak and then it follows a deceleration to zero. The peak varies with the turbulence and rotation conditions. Larger rotation (smaller $Ro$) has smaller inverse energy transfer rate.

In addition to providing evidence to confirm the analytical predictions for scaling of energy decay and inverse energy transfer in DIT, we conclude the effects of a rotating frame of reference on the turbulence development in two aspects. First, rotation prohibits turbulent energy decay, larger rotation, results in slower decay. Second, rotation alters the scaling of inverse energy transfer. While the rotation effect on the energy decay is quite straightforward, its effects on inverse energy transfer are more complex. The effect depends on the range of Fourier mode with which the initial turbulence is input. From the largest $Re_\lambda$ (=255) and smallest $Ro$ (=0.8) this study was conducted with a resolution of $256^3$, and the quantitative evaluation of such effects is available. We propose further study using higher resolution such as $512^3$ or even $1024^3$, thus much higher value of $Re_\lambda$ and much lower value of $Ro$ can be achieved We will be able to explore deeper physics about if and/or how rotation also prohibits inverse energy transfer. Meanwhile, it was recently shown that the truncation at low wave numbers always yields large-scale anisotropy by the discrete Fourier transform is introduced and such anisotropy can be efficiently reduced by simply damping the low-wave-number energies or increasing the energy-containing wave number [51,52]. We will put these numerical effects into consideration in our further study of the research subject.

## Conflict of Interest

The author(s) declared no potential conflicts of interest with respect to the research, authorship and publication of this article.

## Funding

# References

[1] Batchelor G.K., *The theory of homogeneous turbulence*, Cambridge university press, 1953.

[2] Birkhoff G., Fourier synthesis of homogeneous turbulence. *Communications on Pure and Applied Mathematics.* 7(1), 1954, 19-44.

[3] Batchelor G.K., Proudman I., The large-scale structure of homogeneous turbulence. *Philosophical Transactions of the Royal Society of London A: Mathematical, Physical and Engineering Sciences.* 248(949), 1956, 369-405.

[4] Saffman P.G., The large-scale structure of homogeneous turbulence. *Journal of Fluid Mechanics.* 27(3), 1967, 581-593.

[5] Loitsyansky L.G., Some basic laws for isotopic turbulent flows. *Centr, Aero. Hydrodyn. Inst. Rep. No.440.* 1939,

[6] Ishida T., Davidson P.A., Kaneda Y., On the decay of isotropic turbulence. *Journal of Fluid Mechanics.* 564, 2006, 455-475.

[7] Pope S.B., *Turbulent flows*, Cambridge university press, 2000.

[8] Clark T.T., Zemach C., Symmetries and the approach to statistical equilibrium in isotropic turbulence. *Physics of Fluids.* 10(11), 1998, 2846-2858.

[9] Teitelbaum T., Mininni P.D., The decay of turbulence in rotating flows. *Physics of Fluids.* 23(6), 2011, 065105.

[10] Cambon C., Jacquin L., Spectral approach to non-isotropic turbulence subjected to rotation. *Journal of Fluid Mechanics.* 202, 1989, 295-317.

[11] Waleffe F., Inertial transfers in the helical decomposition. *Physics of Fluids A: Fluid Dynamics.* 5(3), 1993, 677-685.

[12] Jacquin L., Leuchter O., Cambonxs C., Mathieu J., Homogeneous turbulence in the presence of rotation. *Journal of Fluid Mechanics.* 220, 1990, 1-52.

[13] Bartello P., Métais O., Lesieur M., Coherent structures in rotating three-dimensional turbulence. *Journal of Fluid Mechanics.* 273, 1994, 1-29.

[14] Müller W.C., Thiele M., Scaling and energy transfer in rotating turbulence. *Europhysics Letters.* 77(3), 2007, 34003.

[15] Bokhoven L.J.A.V., Cambon C., Liechtenstein L., Godeferd F.S., Clercx H.J.H., Refined vorticity statistics of decaying rotating three-dimensional turbulence. *Journal of Turbulence.* 9(6), 2008, 1-24.

[16] Mininni P.D., Pouquet A., Helicity cascades in rotating turbulence. *Physical Review E.* 79(2), 2009, 026304.

[17] Morize C., Moisy F., Rabaud M., Decaying grid-generated turbulence in a rotating tank. *Physics of Fluids.* 17(9), 2005, 095105.

[18] Morize C., Moisy F., Energy decay of rotating turbulence with confinement effects. *Physics of Fluids.* 18(6), 2006, 065107.

[19] Richardson L.F., *Weather prediction by numerical process*, Cambridge University Press, 1922.

[20] Kraichnan R.H., Montgomery D., Two-dimensional turbulence. *Rep. Prog. Phys.* 43,1980,

[21] Tabeling P., Two-dimensional turbulence: a physicist approach. *Physics Reports.* 362(1), 2002, 1-62.

[22] Xia H., Punzmann H., Falkovich G., Shats M.G., Turbulence-condensate interaction in two dimensions. *Physical review letters.* 101(19), 2008, 194504.

[23] Baggaley A.W., Barenghi C.F., Sergeev Y.A., Three-dimensional inverse energy transfer induced by vortex reconnections. *Physical Review E.* 89(1), 2014, 013002.

[24] Galanti B., Sulem P.L., Inverse cascades in three-dimensional anisotropic flows lacking parity invariance. *Physics of Fluids A: Fluid Dynamics.* 3(7), 1991, 1778-1784.

[25] Hefer D., Yakhot V., Inverse energy cascade in a time-dependent flow. *Physics of Fluids A: Fluid Dynamics.* 1(8), 1989, 1383-1386.

[26] Yakhot V., Pelz R., Large-scale structure generation by anisotropic small-scale flows. *Physics of Fluids.* 30(5), 1987, 1272-1277.

[27] Yakhot V., Sivashinsky G., Negative-viscosity phenomena in three-dimensional flows. *Physical Review A.* 35(2), 1987, 815.

[28] Waite L.M., Bartello P., The transition from geostrophic to stratified turbulence. *J. Fluid Mech.* 568, 2006, 89-108.

[29] Mininni P.D., Pouquet A., Rotating helical turbulence. I. Global evolution and spectral behavior. *Physics of Fluids.* 22(3), 2010, 035105.

[30] Pouquet A., Sen A., Rosenberg D., Mininni P.D., Baerenzung J., Inverse cascades in turbulence and the case of rotating flows. *Physica Scripta.* 2013, 2013, 014032.

[31] Smith L.M., Waleffe F., Transfer of energy to two-dimensional large scales in forced, rotating three-dimensional turbulence. *Physics of fluids.* 11, 1999, 1608-1622.

[32] Biferale L., Musacchio S., Toschi F., Inverse energy cascade in three-dimensional isotropic turbulence. *Physical review letters.* 108(16), 2012, 164501.

[33] Chen H., Chen S., Matthaeus W.H., Recovery of the Navier-Stokes equations using a lattice-gas Boltzmann method. *Physical Review A.* 45(8), 1992, R5339.

[34] Qian Y.H., Dhumieres D., Lallemand P., Lattice Boltzmann Model for Navier-Stokes Equation. *Europhysics Letters.* 17, 1992, 479-484.

[35] Yu H., Girimaji S.S., Luo L.S., DNS and LES of decaying isotropic turbulence with and without frame rotation using lattice Boltzmann method. *Journal of Computational Physics.* 209(2), 2005, 599-616.

[36] Yu H., Girimaji S.S., Luo L.S., Lattice Boltzmann simulations of decaying homogeneous isotropic turbulence. *Physical Review E*. 71(1), 2005, 016708.

[37] Yu H., Chen R., Wang H., Yuan Z., Zhao Y., An Y.*, et al.*, GPU accelerated lattice Boltzmann simulation for rotational turbulence. *Computers & Mathematics with Applications*. 67(2), 2014, 445-451.

[38] Chen S., Doolen G.D., Lattice Boltzmann method for fluid flows. *Annual review of fluid mechanics*. 30(1), 1998, 329-364.

[39] Aidun C.K., Clausen J.R., Lattice-Boltzmann Method for Complex Flows. *Annual Review of Fluid Mechanics*. 2010, 439-472.

[40] Wang Z., Zhao Y., Sawchuck A.P., Dalsing M.C., Yu H., GPU acceleration of Volumetric Lattice Boltzmann Method for patient-specific computational hemodynamics. *Computers & Fluids*. 115, 2015, 192-200.

[41] Mei R., Shyy W., Yu D., Luo L.S., Lattice Boltzmann method for 3-D flows with curved boundary. *Journal of Computational Physics*. 161(2), 2000, 680-699.

[42] He X.Y., Luo L.S., Lattice Boltzmann model for the incompressible Navier–Stokes equation. *Journal of statistical Physics*. 88(3), 1997, 927-944.

[43] Luo L.S., Theory of the lattice Boltzmann method: Lattice Boltzmann models for nonideal gases. *Physical Review E*. 62(4), 2000, 4982.

[44] Chapman S., Cowling T.G., *The mathematical theory of non-uniform gases: an account of the kinetic theory of viscosity, thermal conduction and diffusion in gases*, Cambridge university press, 1970.

[45] Miyauchi T., Ishizu T., Direct Numerical Simulation of Homogeneous Turbulence (Decay of Passive Scalar Fluctuation). *Trans. JSME*. 57(544), 1991, 4085-4091.

[46] Mansour N.N., Wray A.A., Decay of isotropic turbulence at low Reynolds number. *Physics of Fluids*. 6(2), 1994, 808-814.

[47] Djenidi L., Kamruzzaman M., Antonia R.A., Power-law exponent in the transition period of decay in grid turbulence. *Journal of Fluid Mechanics*. 779, 2015, 544-555.

[48] Burattini P., Lavoie P., Agrawal A., Djenidi L., Antonia R.A., Power law of decaying homogeneous isotropic turbulence at low Reynolds number. *Physical Review E*. 73(6), 2006, 066304.

[49] Kamruzzaman M., Djenidi L., Antonia R.A., Effects of low Reynolds number on decay exponent in grid turbulence. *Procedia Engineering*. 90, 2014, 327-332.

[50] Yamazaki Y., Kaneda Y., Rubinstein R., Dynamics of inviscid truncated model of rotating turbulence. *Journal of the Physical Society of Japan*. 71(1), 2002, 81-92.

[51] Fang L., Background scalar-level anisotropy caused by low-wave-number truncation in turbulent flows. *Physical Review E*. 95(3), 2017, 033102.

[52] Qin Z., Fang L., Fang J., How isotropic are turbulent flows generated by using periodic conditions in a cube? *Physics Letters A*. 380(13), 2016, 1310-1317.